Chemical Engineering Journal 489 (2024) 151141

Contents lists available at ScienceDirect

Chemical Engineering Journal

journal homepage: www.elsevier.com/locate/cej

A novel photoelectrochemical biosensing platform utilizing dual Type-II $Bi_2O_3/CdLa_2S_4/Bi_2S_3$ ternary heterojunctions as signal transduction materials and Cu_2O nanosphere as a sensitizer for CA15-3 detection

Yong Hao [a], Yingying Zhang [a], Xiaodi Zhu [a], Jingui Chen [a], Na Song [a], Huan Wang [a], Nuo Zhang [a], Dawei Fan [a], Hongmin Ma [a,*], Qin Wei [a,b,*], Huangxian Ju [a,c]

[a] Key Laboratory of Interfacial Reaction & Sensing Analysis in Universities of Shandong, School of Chemistry and Chemical Engineering, University of Jinan, Jinan 250022, Shandong, China
[b] Department of Chemistry, Sungkyunkwan University, Suwon 16419, Republic of Korea
[c] State Key Laboratory of Analytical Chemistry for Life Science, Department of Chemistry, Nanjing University, Nanjing 210023, Nanjing, China

ARTICLE INFO

Keywords:
Photoelectrochemical sensor
Dual type-II heterojunction
CA15-3
Cu_2O

ABSTRACT

Sensitive detection of CA15-3 is important for postoperative monitoring and early diagnosis of breast cancer. In this work, a photoelectrochemical (PEC) biosensing platform was constructed of CA15-3 by using $Bi_2O_3/CdLa_2S_4/Bi_2S_3$ ternary type-II heterojunction as the photoactive transduction material for sensitive detection, and the raspberry-shaped Cu_2O nanospheres were exploited as the signal sensitizing tags. On one hand, the use of Bi_2S_3 as a sensitizer can effectively enhance the visible light excitation of the substrate material. On the other hand, Bi_2S_3 and $Bi_2O_3/CdLa_2S_4$ have the ability to create dual type-II heterojunctions with matched energy levels, which significantly enhances the separation and migration efficiency of the photogenerated carriers and effectively suppresses the recombination of the e^-/h^+ pairs. Raspberry-like semiconducting Cu_2O nanospheres can mediate the PEC process of the heterojunctions. An immunosensor was developed combining the signal transduction capacity of ternary heterojunction and the signal sensitizing effect of Cu_2O nanospheres. The proposed PEC immunosensor showed good selectivity and stability for detecting CA15-3 (0.001 ~ 100 U/mL) with a detection limit of 0.0003 U/mL (S/N = 3). The constructed PEC immunosensor had potential applications in the clinical detection of CA15-3, and was expected to play a great role in the early diagnosis of breast cancer in the future. Moreover, in the design engineering of photoactive materials, the improvement of visible excitation and the enhancement of carrier separation efficiency have been realized simultaneously using a single material, which provides new ideas for the design of photoactive materials.

1. Introduction

Nowadays, the incidence of various types of cancer is on the rise due to the serious aging of the population, poor living habits, environmental pollution, and other factors. CA15-3, as an antigen associated with malignant tumors, was often used in the clinical diagnosis of a variety of cancers, including lung cancer and breast cancer [1–3]. Therefore, realizing the rapid and sensitive detection of CA15-3 is of great significance for the early detection of cancers, clinical diagnosis and treatment, as well as treatment prognosis [4,5]. Common methods for the detection of CA15-3 include electrochemiluminescent sensors [6], LSPR biosensors [7], and fluorescent aptamer sensors [8]. Photoelectrochemical (PEC) sensing, an important branch of electrochemical detection, has technical advantages including low cost, high sensitivity, and ease of operation. Now, PEC sensors have been widely used for the detection of disease markers and environmental pollutants [9]. Photoactive materials play a crucial role in PEC sensors, so the rational design of photoactive materials is a key step in the design of high-performance PEC sensors [10].

Photogenerated electron-hole pairs are produced when a photoactive material is excited by visible light. But the photogenerated electron-hole pairs will be compounded in various ways during the migration process,

* Corresponding authors at: Key Laboratory of Interfacial Reaction & Sensing Analysis in Universities of Shandong, School of Chemistry and Chemical Engineering, University of Jinan, Jinan 250022, Shandong, China (Qin Wei).
E-mail addresses: chm_mahm@ujn.edu.cn (H. Ma), sdjndxwq@163.com (Q. Wei).

https://doi.org/10.1016/j.cej.2024.151141
Received 2 January 2024; Received in revised form 3 March 2024; Accepted 7 April 2024
Available online 9 April 2024
1385-8947/© 2024 Elsevier B.V. All rights reserved.

and thus compounding is essentially a key factor affecting the conversion efficiency of photoactive materials [11]. For this reason, researchers have developed different strategies to suppress charge carrier compounding, among which designing and constructing heterojunctions is the most common and effective method because the separation and transfer of photogenerated carriers can be more efficient in the interfacial region of different components. Compared with the binary heterojunction, the ternary heterojunction with reasonable energy band structure can realize sufficient light absorption, effective photoinduced charge separation, and efficient continuous directional electron transfer. From the existing research results, such as WO_3/FeOOH/Cu_2O [12], ZnSe-GCN-MoS_2 [13], UiO-66/NH_2-MIL-125/g-C_3N_4 [14], etc., the photocurrent response of a ternary heterojunction can be improved by at least 50 ~ 100 % compared to the binary heterojunction of which it is composed. However, applications based on the ternary heterojunction are mostly focused on photocatalysis, and less in photoelectrochemistry sensors. Higher photocurrent response can bring wider detection range and higher sensitivity to photoelectrochemical sensors. Therefore, it is meaningful work to design and construct ternary heterojunctions and apply them to photoelectrochemical sensors.

Bi_2O_3 is a semiconductor material with good stability under acid-base conditions [15]. In addition, it has the advantages of simple preparation, low cost, and unique electronic structure [16]. However, bismuth oxide alone has a wide bandgap that makes it difficult for electrons to leapfrog. In past studies, researchers had usually used methods such as constructing heterojunctions [17] or surface modifications [18] to solve this problem. $CdLa_2S_4$ is a ternary sulfide semiconductor material, that has been widely used in environmental purification, energy storage and conversion, and photocatalytic hydrogen production due to its suitable band gap and strong absorption in the visible region [19–21]. The suitable band gap width and perfect band-matching structure of $CdLa_2S_4$ make it one of the best candidates for forming heterojunctions with Bi_2O_3. To improve the photocurrent response of the substrate material, Bi_2S_3 was utilized. Bi_2S_3 is a binary sulfide semiconductor with a narrow bandgap and a wide spectral absorption range, capable of absorbing light up to 800 nm wavelengths [22]. For a sensor, its ultimate goal is to achieve sensitive detection of the object to be measured, to produce a highly sensitive response to trace changes. To achieve this effect, Cu_2O was chosen as the signal tag to realize the signal amplification of the sensor. Cu_2O is a p-type semiconductor material that is simple to synthesize, has a diverse and controllable morphology [23], and possesses an anti-fluorite crystal structure and a direct band gap of 2 ~ 2.2 eV [24,25]. It is widely used in photocatalysis because of its narrow band gap and suitable conduction and valence band energies.

In this study, a dual type-II ternary heterojunction with good photocurrent response was constructed using Bi_2O_3, $CdLa_2S_4$, and Bi_2S_3. Compared with binary heterojunctions, ternary heterojunctions with matched energy band structures are more favorable for improving the visible light absorption and the separation efficiency of photogenerated carriers [26,27]. It is noteworthy that Bi_2S_3 exists as a special presence, which can act as a sensitizer for surface sensitization of Bi_2O_3/$CdLa_2S_4$ to improve visible excitation while forming a ternary heterojunction to improve the carrier separation efficiency. Raspberry-shaped Cu_2O nanospheres were synthesized for the first time. The morphology possesses a larger specific surface area, providing more active loading sites. Cu_2O was used as the signal tag to label the signal antibody, and Cu_2O increased the spatial resistance of the sensor while competing with the substrate for electron donor (AA) and light, resulting in higher sensitivity of the constructed sensor. On this basis, a novel PEC immunosensor was successfully constructed for the sensitive detection of CA15-3. This sensor had potential applications in the detection of CA15-3 and was expected to play a great role in the clinical diagnosis of breast cancer in the future.

2. Experimental section

2.1. Materials and instruments

All reagents and apparatus were reported in the Supporting Information.

2.2. Preparation of $CdLa_2S_4$, Bi_2O_3/$CdLa_2S_4$, Bi_2S_3, and Cu_2O

Fig. S1 showed the synthesis of $CdLa_2S_4$, Bi_2O_3/$CdLa_2S_4$ and Cu_2O. The method of synthesis has been improved from the existing one [13,28,29]. A more detailed synthesis process was reported in the Supporting Information.

2.3. Preparation of Cu_2O-Ab_2 bio-complexes

At first, ethanol(80 mL), water(20 mL), and concentrated ammonia solution (1 mL, 28 wt%) were mixed with 0.1 g of Cu_2O and dispersed by sonication. Subsequently, (3-Aminopropyl) triethoxysilane (APTES, 67 μL) and tetraacetoxysilane (TEOS, 67 μL) were added, and the mixture was stirred for 3 h at 35 degrees Celsius. After undergoing centrifugal drying, aminoconjugated raspberry-like Cu_2O nanorods (Cu_2O-NH_2) were produced. To prepare Cu_2O-Ab_2, 10 μL of Ab_2 solution (10 μg/mL) was mixed with 80 μL of EDC solution (5 mg/mL) and 80 μL of NHS solution (1 mg/mL) and shaken for 30 min. Next, 1 mL of Cu_2O-NH_2 solution (2 mg/mL) was added to the mixture, which was then shaken overnight at 4 °C. The resulting mixture was washed twice by centrifugation: the first time without any additional reagents, and the second time with 1 mL of phosphate-buffered saline (PBS) (0.1 M, pH = 7.4). Finally, the mixture was combined with phosphate-buffered saline to obtain Cu_2O-Ab_2.

2.4. Construction of PEC immunosensor

The ITO conductive glass is first cut to size and pre-treated. Then, 10 μL of Bi_2O_3/$CdLa_2S_4$ suspension (4 mg/mL) was dropped on the conductive glass surface and allowed to dry naturally. Subsequently, 7 μL of 0.14 M $Bi(NO_3)_3$ solution and 7 μL of 0.2 M Na_2S solution were added sequentially to generate Bi_2S_3 in situ dropwise and left to dry. Excess Bi_2S_3 was rinsed off using deionized water and dried again. The prepared electrodes were soaked in 1 mg/mL dopamine hydrochloride solution, held at 4 °C for 10 h, washed with deionized water, and dried. The role of this step is to use the quinone functional group in PDA as a cross-linking agent to covalently react with the antibody with amine as the terminal group through the Michael reaction to immobilize the antibody on the substrate material. Next 6 μL of 10 μg/mL capture antibody Ab_1, 3 μL of 1 wt% bovine serum albumin BSA, 6 μL of different concentrations of CA15-3 antigen and 6 μL of 2 mg/mL Cu_2O-Ab_2 droplets were coated onto the electrodes respectively. Finally, electrodes were incubated in a refrigerator at 4 ℃ for 1 h. When the incubation was completed, they were rinsed with PBS and dried for use (Scheme 1).

2.5. Testing of PEC immunosensor

In this study, a conventional three-electrode system (the working electrode is the sensor, the reference electrode is a saturated calomel electrode (SCE), and the counter electrode is a platinum electrode) was used to test. The light source system was a 100 *W* LED lamp, and the PEC signal was detected with a CHI760E electrochemical workstation with an applied voltage of 0 *V* and PBS as a buffer solution.

3. Results and discussion

3.1. Materials characterization

Scanning electron microscopy (SEM) images showed that the

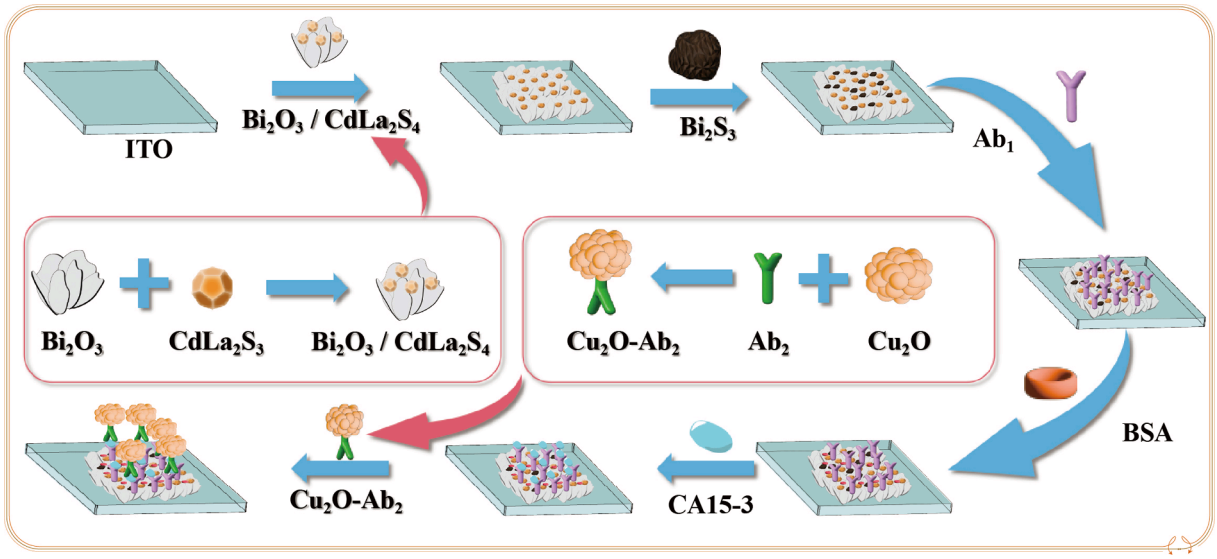

Scheme 1. Construction of PEC immunosensor.

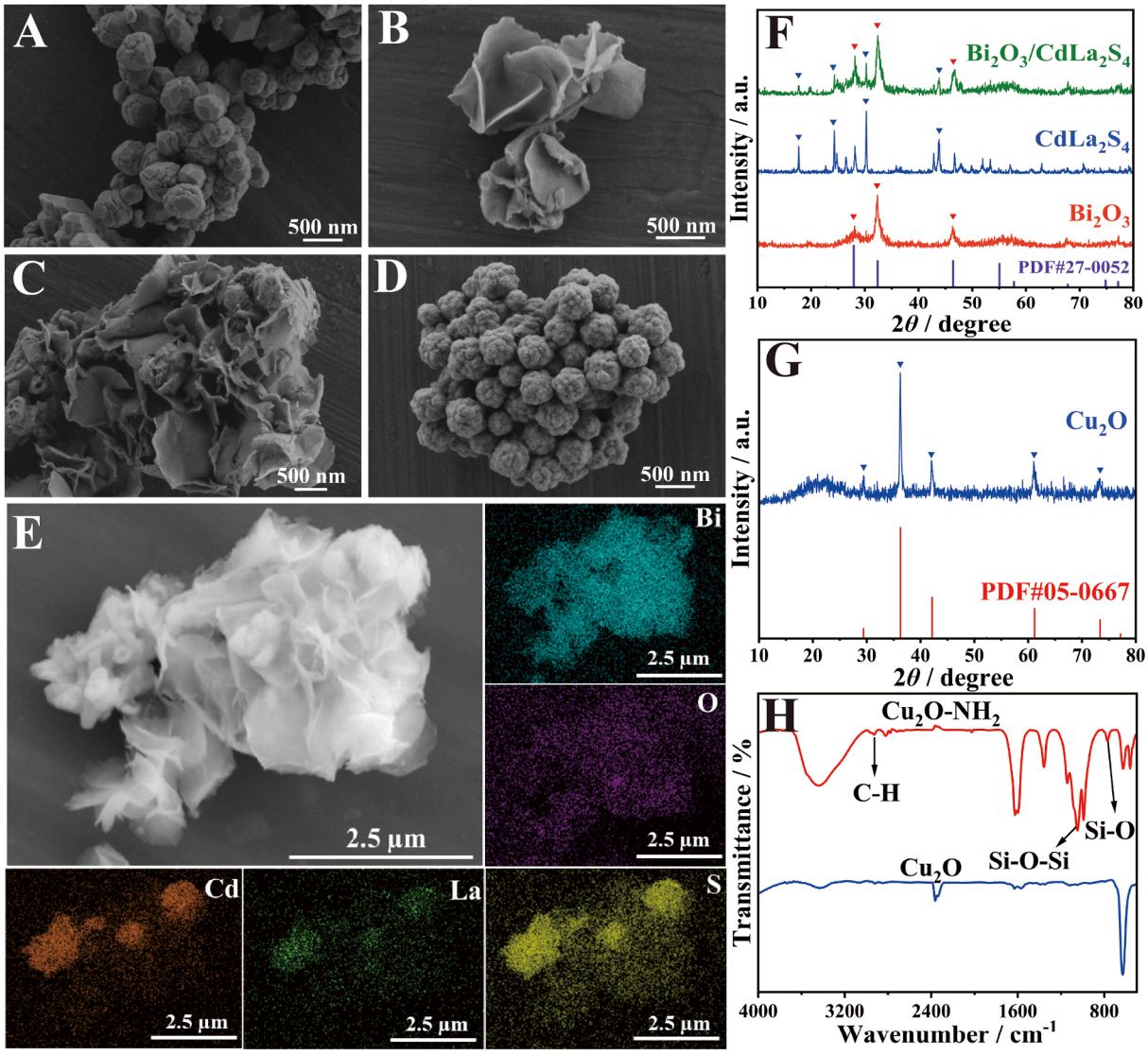

Fig. 1. SEM images of $CdLa_2S_4$ (A), Bi_2O_3 (B), Bi_2O_3/$CdLa_2S_4$ (C) and Cu_2O (D), Elemental mapping images of Bi_2O_3/$CdLa_2S_4$ (E), XRD pattern of Bi_2O_3/$CdLa_2S_4$ (F) and Cu_2O (G), FT-IR spectra of Cu_2O and Cu_2O-NH_2 (H).

morphology of the prepared $CdLa_2S_4$ was Bufon fruit-like nanoparticles with diameters in the range of 400 – 500 nm (Fig. 1A) while Bi_2O_3 was stacked by irregular nanosheets with diameters around 1 μm (Fig. 1B). $CdLa_2S_4$ nanoparticle ensembles were dispersed onto Bi_2O_3-stacked nanosheets to form $Bi_2O_3/CdLa_2S_4$ complexes (Fig. 1C). TEM image of $Bi_2O_3/CdLa_2S_4$ (Fig. S2C) can also further corroborate the successful composite. Image of EDS (Fig. S2E) and Elemental Mapping (Fig. 1E) of $Bi_2O_3/CdLa_2S_4$ showed the distribution locations of the elements Bi, O, S, Cd, and La. Cu_2O synthesized in this study appeared as raspberry-like nanoparticles with diameters of approximately 300 – 400 nm, as shown in Fig. 1D and Fig. S2D using scanning electron microscopy. To demonstrate the successful growth of Bi_2S_3 at the electrode, the electrode surface was compared before and after in situ Bi_2S_3 growth. The results depicted in Fig. S4 demonstrate significant changes in the surface morphology of the electrodes before and after in situ growth of Bi_2S_3, indicating successful generation of Bi_2S_3. In addition, based on SEM images (Fig. S2A), it was determined that Bi_2S_3 does not exhibit any specific morphology.

The XRD Images provide information about the crystal structure and composition of the samples obtained. Fig. 1F showed several different diffraction peaks of $CdLa_2S_4$ [30], which indicates that the synthesized $CdLa_2S_4$ was highly crystalline and had no other phase. And XRD pattern of prepared Bi_2O_3 indicated diffraction of (111), (200), and (220) crystal planes at peaks 27.9, 32.3, and 46.4 respectively, which was in agreement with the standard card PDF#27–0052 [31]. In addition to this, the characteristic peaks of both Bi_2O_3 and $CdLa_2S_4$ can be seen in Fig. 1F in the prepared complexes, which indicated that $Bi_2O_3/CdLa_2S_4$ complexes had been successfully prepared. Fig. 1G confirmed the successful preparation of Cu_2O with good crystallinity, as seen by the characteristic peaks aligned with standard card PDF#05–0667. The XRD image of Bi_2S_3 (Fig. S2B) showed that the position of its peaks was consistent with that of the standard card (PDF#04–0774), indicating successful preparation of Bi_2S_3.

Fourier transform infrared spectroscopy (FT-IR) spectra were used to determine the results of the modification modification of Cu_2O nanospheres by APTES. Fig. 1H demonstrates that compared to the Cu_2O curve, the Cu_2O-NH_2 curve displays three new peaks at wavelengths of approximately 2930 cm^{-1}, 1010 cm^{-1}, and 830 cm^{-1}. These peaks belonged to the stretching vibrational peaks of the C-H, Si-O-Si, and Si-O groups of APTES. It seemed that APTES had successfully enveloped the Cu_2O nanorods.

X-ray photoelectron spectroscopy (XPS) showed the valence states of the elements Bi, O, Cd, La, and S in $Bi_2O_3/CdLa_2S_4$ (Fig. 2A). Fig. 2B shows the peak splitting results of O 1 s with lattice oxygen (Bi-O) at 530.8 eV, and surface adsorbed oxygen (O_{abs}) at 532.1 eV. Fig. 2C indicated that the Bi $4f_{5/2}$ and Bi $4f_{7/2}$ orbitals' peaks were at 159.4 and 165.0 eV, respectively. The peaks of the Cd $3d_{3/2}$ and Cd $3d_{5/2}$ orbitals can be seen in Fig. 2D at 412.6 and 405.5 eV. According to Fig. 2E, the La 3d orbital split into La $3d_{5/2}$ (838.8 eV), La $3d_{5/2}$ (834.8 eV), La $3d_{3/2}$ (852.1 eV) and La $3d_{3/2}$ (854.9 eV). Fig. 2C showed that the binding energies at 160.5 and 165.9 eV should belong to the genus S $2p_{1/2}$ and S $2p_{3/2}$ orbitals, respectively. Subsequently, a comparison of the binding energies before and after the complexation of each element reveals that the binding energies are shifted in a lower direction, which suggests that a strong chemical bond exists between Bi_2O_3 and $CdLa_2S_4$. These results clearly support the formation of $Bi_2O_3/CdLa_2S_4$ heterojunctions.

3.2. Comparison of PEC signals

In order to better compare the positive influence of the ternary heterojunction on the photocurrent response, the photocurrent responses of Bi_2O_3, Bi_2S_3, $CdLa_2S_4$, $Bi_2O_3/CdLa_2S_4$, and $Bi_2O_3/CdLa_2S_4/Bi_2S_3$ were tested under identical conditions Based on Fig. S5, it could be seen that the photocurrent response of pure Bi_2O_3, pure Bi_2S_3, and pure $CdLa_2S_4$ were feeble. The photocurrent responses of $Bi_2O_3/CdLa_2S_4$ and Bi_2O_3/Bi_2S_3 were significantly improved compared to those of the individual materials. This was mainly due to the heterojunction structure which greatly improved carrier separation efficiency. The addition of Bi_2S_3 resulted in a substantial enhancement of the photocurrent response, which suggested that ternary heterojunctions were able to promote rapid carrier separation and migration relative to binary heterojunctions, overcoming the problem of short carrier lifetimes due to photogenerated carrier composite.

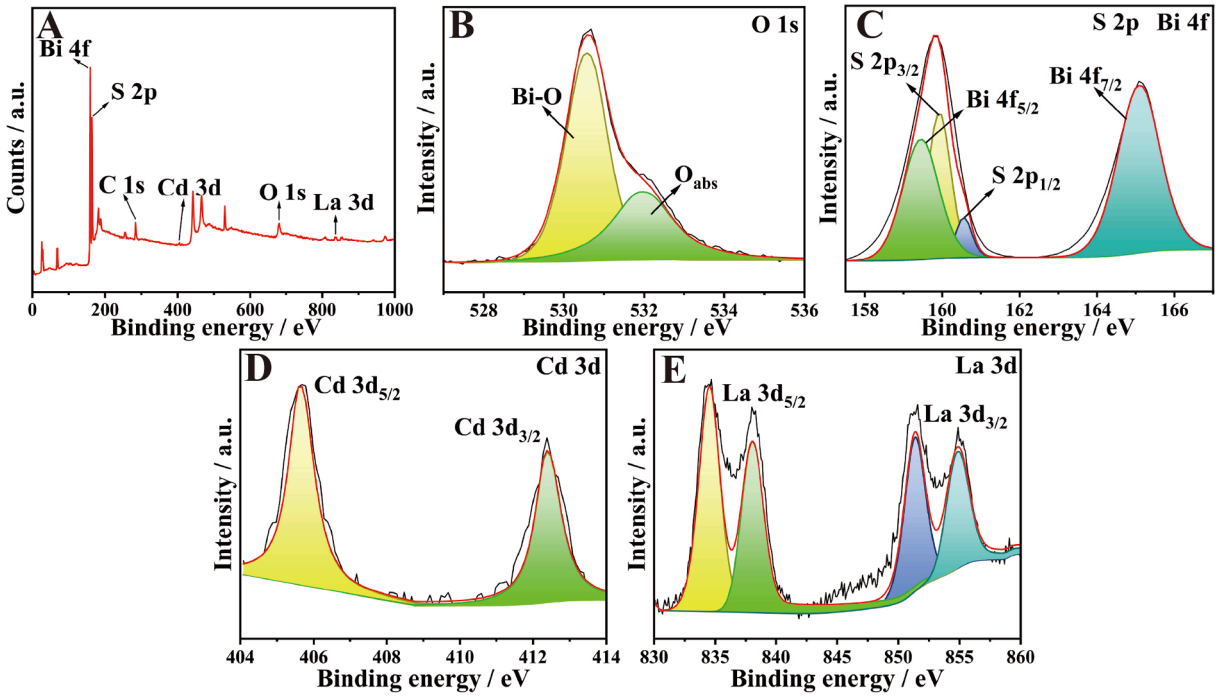

Fig. 2. X-ray photoelectron spectroscopy (XPS) spectra of the $Bi_2O_3/CdLa_2S_4$ heterojunction(A), XPS spectra of O 1 s (B), Bi 4f and S 2p (C), Cd 3d (D), La 3d (E).

3.3. Mechanistic of PEC immunosensors

Using UV–Vis diffuse reflectance spectroscopy (DRS) analysis to study photoactive materials' light absorption properties is effective [32]. Forbidden bandwidths of synthesized Bi_2O_3, $CdLa_2S_4$, Bi_2S_3, and Cu_2O analyzed according to Fig. S6 were respectively about 3.1 eV, 2.2 eV, 1.3 eV, and 1.6 eV. In addition, the type of material can be determined from the Mott-Schottky curve [33], so from the image analysis, it can be learned that Bi_2O_3, $CdLa_2S_4$, Bi_2S_3 are n-type semiconductors, and Cu_2O is a p-type semiconductor. Mott-Schottky curves also can infer flat-band potentials (E_{fb}) of Bi_2O_3, Bi_2S_3, $CdLa_2S_4$, and Cu_2O to be 0.28, −0.71, −0.45, and 1.36 V vs SCE, respectively (Fig. S7). Conduction band potentials (E_{CB}) of Bi_2O_3, Bi_2S_3, and $CdLa_2S_4$ were 0.28, −0.71, and −0.45 V vs SCE, and valence band potential (E_{VB}) of Cu_2O was 1.36 V vs SCE. Based on $Eg = E_{VB} - E_{CB}$, E_{VB} of Bi_2O_3, Bi_2S_3, and $CdLa_2S_4$ were 3.38, 0.59, and 1.75 V vs SCE, and E_{CB} of Cu_2O was 0.24 V vs SCE. Therefore, Bi_2O_3, $CdLa_2S_4$, and Bi_2S_3 could form energy band-matched dual type-II heterojunctions.

Based on the above test results, the working mechanism of the PEC immunosensor could be hypothesized (Fig. 3). Photoreactive materials generate photogenerated electron/hole pairs (e^-/h^+) after visible light irradiation. The presence of sensitizer Bi_2S_3 improves the overall visible excitation of the substrate material. Since Bi_2O_3, $CdLa_2S_4$, and Bi_2S_3 can form a matched energy level structure, the e^- migrated sequentially down the conduction band from Bi_2S_3 to $CdLa_2S_4$, Bi_2O_3, and ultimately to the ITO surface. In contrast, the h^+ were sequentially migrated down the valence band from Bi_2O_3 to $CdLa_2S_4$, Bi_2S_3, and finally captured by the electron donor. The final results showed that the ternary heterojunction composed of $Bi_2O_3/CdLa_2S_4/Bi_2S_3$ significantly enhances the separation efficiency of the carriers and prevented effectively e^-/h^+ pairs complexation. The photoquencher Cu_2O can effectively reduce the photocurrent response for the following possible reasons. On one hand, Cu_2O competed with the substrate material for visible light, and at the same time the h^+ produced by Cu_2O by photoexcitation also competed with the substrate material for electron donors (AA). On the other hand, the prepared raspberry-like Cu_2O had a large specific surface area, which provided abundant active sites for antibody loading. In addition, the spatial site resistance of Cu_2O further reduced the contact between electron donors (AA) and the substrate material, which decreased the efficiency of hole removal by electron donors. Therefore photoquencher Cu_2O was an effective signal amplification strategy. In summary, the electron transfer mechanism of the ternary heterojunction and the mode of action of photoquencher Cu_2O were discussed to provide a theoretical basis for the construction of the sensor.

3.4. EIS and PEC behaviors

When constructing the PEC immunosensor, the signal changes somewhat with each modified layer [34]. Fig. 4A perfectly showed the current variation during the construction of the sensor, and it can be seen that with the construction of the heterojunction, the photocurrent response also peaks at curve c. As Ab_1, BSA, and CA15-3 were modified onto the ITO/Bi_2O_3/$CdLa_2S_4$/Bi_2S_3 electrodes and incubated, the current signals began to diminish gradually, which was attributed to the blocking and spatial site-blocking effects of the proteins (curve e − h). The main reason for the decrease in curve h was the role of the antibody-labeled immune complex (Cu_2O-Ab_2). Notably, there was a small upward increase in the curve d due to the presence of polydopamine. This is because polydopamine can absorb visible light, act as a photosensitizer, and transfer electrons, resulting in higher photocurrent.

EIS is a widely used method for analyzing interfacial properties, and the magnitude of the electron transfer resistance (R_{et}) in the analysis of the results can be expressed in terms of the magnitude of the diameter of the semicircle. The layer-modified electrodes were tested for electrochemical impedance in a solution containing 0.10 M KCl and 5.0 mM $[Fe(CN)_6]^{3-/4-}$. In the Nyquist plot shown in Fig. 4B, it was shown that the semicircle of ITO was very small, indicating a low R_{et}. This was because ITO has good electrical conductivity. The increasing R_{et} values after sequential dropwise addition of Bi_2O_3/$CdLa_2S_4$, Bi_2S_3, Ab_1, BSA, CA15-3, and Cu_2O-Ab_2 on ITO further proved the success of the sensor construction. Exceptionally, a decrease in the value of R_{et} occurred after modification with polydopamine. Data collected from EIS had confirmed that the construction of the PEC immunosensor was successful.

3.5. Comparison of electrode activity area

A larger specific surface area means more active sites, necessitating surface area evaluation of the electrode [35]. Cyclic voltammetry (CV) test was performed on ITO alone, ITO/Bi_2O_3/$CdLa_2S_4$, and ITO/Bi_2O_3/$CdLa_2S_4$/Bi_2S_3 in order to visualize the change in the surface active area of the substrate materials more intuitively. The test was performed in $[Fe(CN)_6]^{4-/3-}$ solution and all analyses were based on the Randles Sevcik equation ($I_p = (2.69 \times 10^5)\, AD^{1/2}n^{3/2}v^{1/2}c$, where I_p is the peak

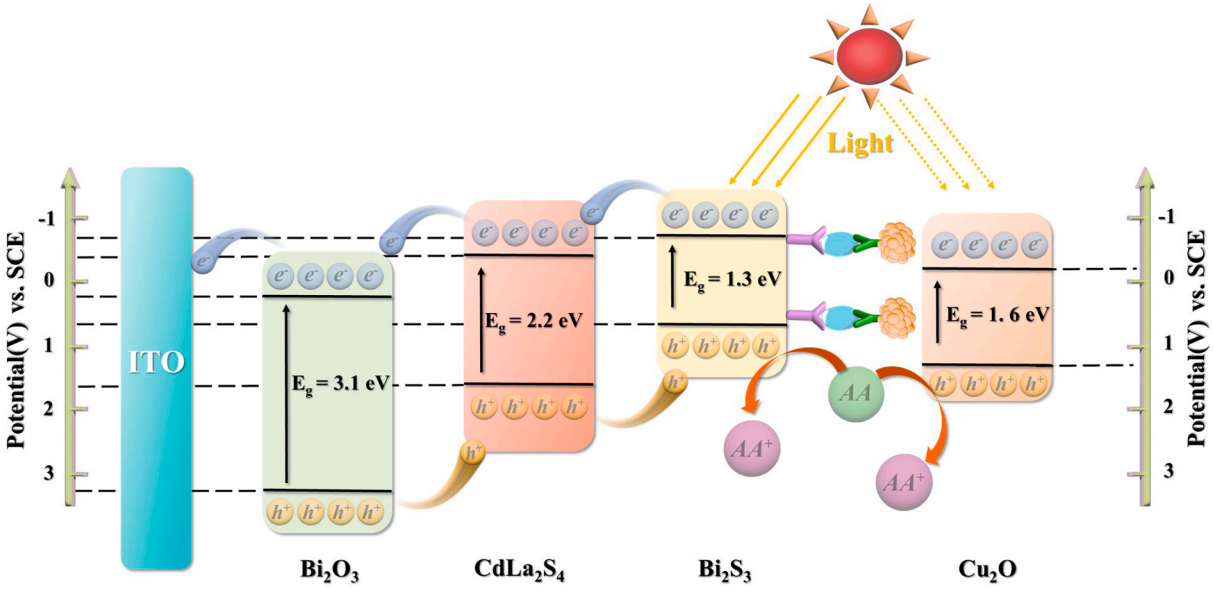

Fig. 3. PEC immunosensor possible mechanism diagram.

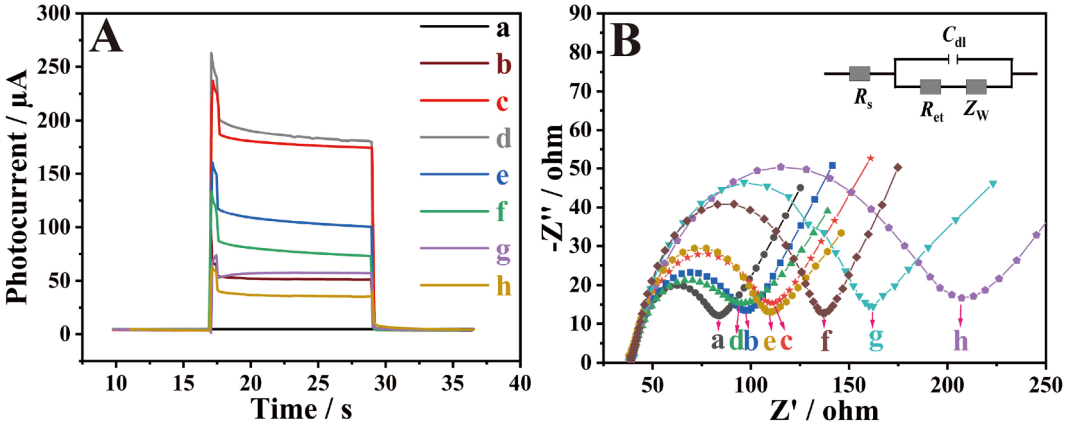

Fig. 4. (A) Photocurrent response and (B) EIS plots:(a) ITO, (b) ITO/Bi_2O_3/$CdLa_2S_4$, (c) ITO/Bi_2O_3/$CdLa_2S_4$/Bi_2S_3, (d) ITO/Bi_2O_3/$CdLa_2S_4$/Bi_2S_3/PDA, (e) ITO/Bi_2O_3/$CdLa_2S_4$/ Bi_2S_3/PDA/Ab_1, (f) ITO/Bi_2O_3/$CdLa_2S_4$/Bi_2S_3/PDA/Ab_1/BSA,(g) ITO/Bi_2O_3/$CdLa_2S_4$/ Bi_2S_3/PDA/Ab_1/BSA/CA15-3, and (h) ITO/Bi_2O_3/$CdLa_2S_4$/ Bi_2S_3/PDA/Ab_1/BSA/ CA15-3/Cu_2O-Ab_2.

current, A is the electroactive surface area of the electrode, D is the value of the $[Fe(CN)_6]^{4-/3-}$ diffusion coefficient of (6.70 ± 0.02) × 10^{-6} cm^2/s, n is 1, which denotes the number of electrons transferred in the redox reaction, c is the value of the concentration of $[Fe(CN)_6]^{4-/3-}$ at 5 mmol/L, and v is the scanning volume CV rate (V/s). Cyclic voltammetry tests were performed on the electrodes at scan rates of 0.1–2.7 V/s, respectively, and the results were shown in Fig. S8. Subsequently the results were linearly fitted and the fitted regression equations were respectively $I_p = 2237\ v^{1/2}$–72 ($R^2 = 0.9965$), $I_p = 2562\ v^{1/2}$–108 ($R^2 = 0.9995$), and $I_p = 3488\ v^{1/2}$–6 ($R^2 = 0.9976$). Taking into account the Randles Sevcik equation, the effective electrochemically active surface area of the ITO alone electrode, the ITO/Bi_2O_3/$CdLa_2S_4$ electrode, and the ITO/Bi_2O_3/$CdLa_2S_4$/Bi_2S_3 electrode can be calculated as 0.64 cm^2, 0.74 cm^2, and 1.00 cm^2. The results showed that the electrochemically active surface area of the modified ITO/Bi_2O_3/$CdLa_2S_4$ nanocomposites increased by 15.6 %, while the electrochemically active surface area of ITO/Bi_2O_3/$CdLa_2S_4$/Bi_2S_3 increased by 35.1 % in comparison to ITO/Bi_2O_3/$CdLa_2S_4$.

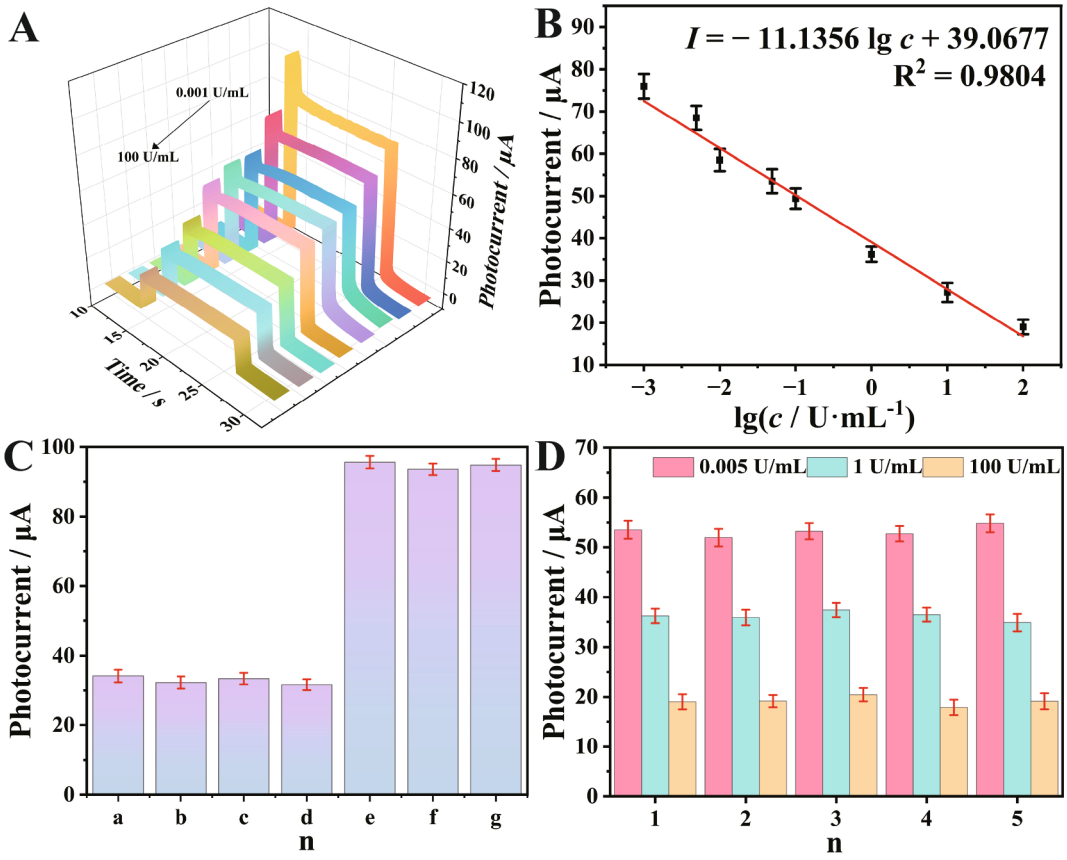

Fig. 5. (A) Photocurrent response of the Bi_2O_3/$CdLa_2S_4$/Bi_2S_3 electrode for detection of CA15-3. (B) The working curve for different CA15-3 concentrations. (C) Selectivity of the PEC immunosensor for CA15-3, CA15-3 (a), CA15-3 and CEA (b), CA15-3 and CYFRA 21–1 (c), CA15-3 and NSE (d), CEA alone (e), CYFRA 21–1 alone (f), and NSE alone (g). (D) repeatability test of PEC immunosensor with CA15-3 concentrations.

3.6. Condition optimization

The performance of the PEC immunosensor is affected by several external factors, so the external conditions were screened to obtain the optimal experimental conditions [36,37]. The pH of PBS in the buffer and the concentration of the electron donor (AA) were first screened, and the photocurrent response peaked when the AA concentration was 0.1 mol/L and the pH of PBS was 7.4, as shown in Fig. S9A and Fig. S9B. The mass ratio of the two in the $Bi_2O_3/CdLa_2S_4$ complex was then screened, as shown in Fig. S9C, and the sensor photocurrent was maximum when the mass ratio of Bi_2O_3 to $CdLa_2S_4$ was 1:1.3. The volumes of the $Bi(NO_3)_3$ and Na_2S solutions used for in situ growth of Bi_2S_3 were subsequently optimized. The screening process, as shown in Fig. S9D, revealed the optimal sensor photocurrent when the volume of the solution was 7 μL. Finally, the incubation time of Cu_2O-Ab_2 was optimized. The results showed that there was almost no change in the photocurrent response when the incubation time exceeded 1 h (Fig. S9E). Therefore, 1 h was recognized as the optimal incubation time.

3.7. Immunosensor performance

After optimizing experimental conditions, PEC immunosensor was used to analyze different concentrations of CA15-3. As can be seen from Fig. 5A and Fig. 5B, the photocurrent was negatively related to CA15-3 concentration, and logarithmic value of photocurrent response and CA15-3 concentration was linear. Fig. 5B showed the fitting results, the linear regression equation is $I = -11.1356 \lg c + 39.0677$ (where I (μA) is the photocurrent, c (U/mL) is the CA15-3 concentration), and the square of the correlation coefficient $R^2 = 0.9804$. Finally, the detection limit of the fabricated sensor was calculated to be 0.0003 U/mL. The sensor constructed by this method had a wider detection range and lower detection line compared to other methods for CA15-3 detection (Table S1).

3.8. Selectivity, Repeatability, and stability of sensor

It is critical to analyze the performance of the sensors to ensure the reliability of the serum sample detection [38–40]. Therefore, the selectivity, repeatability, and stability of the constructed sensors were examined. Firstly, the PEC immunosensor's selectivity was tested by measuring its response to CA15-3, a combination of CA15-3 and interfering antibodies, and interfering antibodies alone. According to the experimental results shown in Fig. 5C, the sensor had excellent selectivity. To check the repeatability of the sensor, five electrodes were utilized to detect different concentrations of CA15-3. As shown in Fig. 5D, the photocurrent response fluctuated less among electrodes with RSD values of 2.0 %, 2.6 %, and 4.7 % at the same concentration. After being irradiated by switching the light on and off 20 times in 400 s when the concentration of CA15-3 was 1 U/mL, the PEC immunosensor exhibited good stability, as shown in Fig. S10A. Next, the storage stability was examined. Based on the data presented in Fig. S10B, it can be observed that two sets of electrodes with varying concentrations showed photocurrent signals that still were 95.1 % and 92.3 % of the initial signals after 16 days of being stored in a refrigerator at 4 °C. This suggested that the sensor had good storage stability.

3.9. Sample analysis

Using the standard addition method, the sensor was tested for feasibility and accuracy in analyzing real serum samples. As shown in Table 1, CA15-3 standard solutions of 2.00, 5.00, and 7.00 U/mL were added dropwise to the samples, respectively. The RSD of CA15-3 samples were in the range of 1.5 ~ 2.1 %, and the spiked recoveries were 104.50, 97.60, and 102.43 %, respectively. To further assess the usability of the sensor, five sets of serum samples were chosen and the readings obtained from this method (Y) were compared with those from the Beckman Automated CL Analyzer-Access IA system (X) (Table 2). The regression equation derived from the comparison was $Y = 1.0520*X - 2.4362$ (with $R^2 = 0.9981$). This indicates a high level of correlation between the two systems, thus validating the usefulness of the constructed sensor. Therefore, the PEC biosensing platform has good application prospects in serum sample analysis.

Table 1
The results of the CA15-3 determination in samples.

Samples (U/mL)	Addition (U/mL)	Average (U/mL, n = 5)	RSD (%, n = 5)	Recovery (%)
4.69	2.0	6.78	2.1	104.50
	5.0	9.57	1.5	97.60
	7.0	11.86	1.7	102.43

4. Conclusion

In this study, through the rational design of the photoactive materials, the visible light excitation is improved and the carrier separation efficiency is enhanced, so that the photocurrent of the final substrate material obtains a significant enhancement accordingly. A dual type-II photoelectrochemical biosensing platform was developed to realize the sensitive detection of CA15-3 by using $Bi_2O_3/CdLa_2S_4/Bi_2S_3$ dual type-II heterojunction as the photoactive substrate material and raspberry-shaped Cu_2O nanorods were synthesized for the first time as the light quencher. The dual type-II $Bi_2O_3/CdLa_2S_4/Bi_2S_3$ heterojunction provided excellent photocurrent response. The large spatial site resistance and strong competitiveness of the raspberry-like Cu_2O endowed the sensor with high sensitivity. The PEC biosensing platform was able to detect CA15-3 in the range of 0.001 ~ 100 U/mL with a limit of detection of 0.0003 U/mL. Moreover, the experimental results showed that the constructed PEC immunosensor had good selectivity, repeatability, and stability. This sensor had potential applications in the detection of CA15-3 and was expected to play a great role in the future clinical diagnosis of breast cancer.

CRediT authorship contribution statement

Yong Hao: Writing – original draft, Data curation. **Yingying Zhang:** Software, Resources. **Xiaodi Zhu:** Validation, Supervision. **Jingui Chen:** Resources, Methodology. **Na Song:** Project administration, Investigation. **Huan Wang:** Formal analysis, Conceptualization. **Nuo Zhang:** Validation, Software. **Dawei Fan:** Project administration, Methodology. **Hongmin Ma:** Funding acquisition, Formal analysis. **Qin Wei:** Software, Project administration, Methodology. **Huangxian Ju:** Supervision, Formal analysis.

Declaration of competing interest

The authors declare that they have no known competing financial interests or personal relationships that could have appeared to influence the work reported in this paper.

Table 2
Analytical results of human serum samples.

Number of human sera samples	Average (U/mL, n = 5)	RSD (%, n = 5)	Beckman Analyzer (U/mL)
1	13.5	7.5	12.1
2	19.7	7.2	18.0
3	35.6	6.8	33.7
4	53.6	6.3	55.8
5	88.6	5.7	90.2

Data availability

Data will be made available on request.

Acknowledgments

This work was financially supported by the National Natural Science Foundation of China (22374059), the Shandong Provincial Natural Science Foundation (ZR2020YQ13), a Project of Shandong Province Higher Educational Youth Innovation Science and Technology Program (2020KJC008). Ma and Wei thank the Taishan Scholars Program of Shandong Province of China.

Appendix A. Supplementary data

Supplementary data to this article can be found online at https://doi.org/10.1016/j.cej.2024.151141.

References

[1] X. Jiang, H. Wang, R. Yuan, Y. Chai, Sensitive electrochemiluminescence detection for CA15-3 based on immobilizing luminol on dendrimer functionalized ZnO nanorods, Biosens. Bioelectron. 63 (2015) 33–38, https://doi.org/10.1016/j.bios.2014.07.009.

[2] S. Akbari Nakhjavani, B. Khalilzadeh, P. Samadi Pakchin, R. Saber, M. H. Ghahremani, Y. Omidi, A highly sensitive and reliable detection of CA15-3 in patient plasma with electrochemical biosensor labeled with magnetic beads, Biosens. Bioelectron. 122 (2018) 8–15, https://doi.org/10.1016/j.bios.2018.08.047.

[3] M. Hasanzadeh, S. Tagi, E. Solhi, N. Shadjou, A. Jouyban, A. Mokhtarzadeh, Immunosensing of breast cancer prognostic marker in adenocarcinoma cell lysates and unprocessed human plasma samples using gold nanostructure coated on organic substrate, Int. J. Biol. Macromol. 118 (Pt A) (2018) 1082–1089, https://doi.org/10.1016/j.ijbiomac.2018.06.091.

[4] X.Y. Ge, Y.G. Feng, S.Y. Cen, A.J. Wang, L.P. Mei, X. Luo, J.J. Feng, A label-free electrochemical immnunosensor based on signal magnification of oxygen reduction reaction catalyzed by uniform PtCo nanodendrites for highly sensitive detection of carbohydrate antigen 15–3, Anal. Chim. Acta 1176 (2021) 338750, https://doi.org/10.1016/j.aca.2021.338750.

[5] S. Song, N. Li, L. Bai, P. Gai, F. Li, Photo-assisted robust anti-interference self-powered biosensing of MicroRNA based on Pt-S Bonds and the inorganic-organic hybridization strategy, Anal. Chem. 94 (3) (2022) 1654–1660, https://doi.org/10.1021/acs.analchem.1c04135.

[6] D. Qin, X. Jiang, G. Mo, J. Feng, C. Yu, B. Deng, A novel carbon quantum dots signal amplification strategy coupled with sandwich electrochemiluminescence immunosensor for the detection of CA15-3 in human serum, ACS Sens. 4 (2) (2019) 504–512, https://doi.org/10.1021/acssensors.8b01607.

[7] Z. Fan, Z. Geng, W. Fang, X. Lv, Y. Su, S. Wang, H. Chen, Smartphone biosensor system with multi-testing unit based on localized surface plasmon resonance integrated with microfluidics chip, Sensors (basel) 20 (2) (2020), https://doi.org/10.3390/s20020446.

[8] W. Hu, Y. Wang, M. Qian, L. Wang, Y. Dong, A. Label-free, "Lock-key" Fluorescence Aptasensing Based on Triplex-helix DNA and G-quadruplex for CA15-3 Detection, Anal. Sci. 37 (6) (2021) 905–909, https://doi.org/10.2116/analsci.20P332.

[9] D. Zheng, J. Yang, Z. Zheng, M. Peng, J. Chen, Y. Chen, W. Gao, A highly sensitive photoelectrochemical biosensor for CEA analysis based on hollow NiS@NiO/TiO_2 composite with typal p-n heterostructure, Talanta 246 (2022) 123523, https://doi.org/10.1016/j.talanta.2022.123523.

[10] J. Wang, J. Xie, M. Chen, S. Zheng, H. Tan, S. Yu, Y. Chen, X. Huang, W. Gao, Core-double-shell structure and heterojunction in CdS/SnS_2 boosting fast carrier separation for ultrasensitive detection of carbohydrate antigen 125, Sensor. Actuat. B-Chem. 380 (2023) 133352, https://doi.org/10.1016/j.snb.2023.133352.

[11] J. Shu, D. Tang, Recent advances in photoelectrochemical sensing: from engineered photoactive materials to sensing devices and detection modes, Anal. Chem. 92 (1) (2019) 363–377, https://doi.org/10.1021/acs.analchem.9b04199.

[12] P. Wang, Z. Hao, Z. Liu, FeOOH interlayer with storing holes applied to construct WO_3/FeOOH/Cu_2O ternary heterojunction photoanode with dual built-in electric filed for efficient PEC cell, J. Alloys. Compd. 917 (2022) 165496, https://doi.org/10.1016/j.jallcom.2022.165496.

[13] E. Sitara, H. Nasir, S. Iram, S.A.B. Bukhari, T. Akhtar, S. Mumtaz, Tailoring of ZnSe/GCN/MoS_2 ternary heterojunction with enhanced photoelectrochemical activity for water oxidation, Surf. Interfaces. 37 (2023) 102632, https://doi.org/10.1016/j.surfin.2023.102632.

[14] H. Sepehrmansourie, H. Alamgholiloo, N. Noroozi Pesyan, M.A. Zolfigol, A MOF-on-MOF strategy to construct double Z-scheme heterojunction for high-performance photocatalytic degradation, Appl. Catal. B-Environ. (2023) 122082, https://doi.org/10.1016/j.apcatb.2022.122082.

[15] T. Xie, C. Liu, L. Xu, J. Yang, W. Zhou, Novel heterojunction Bi_2O_3/$SrFe_{12}O_{19}$ magnetic photocatalyst with highly enhanced photocatalytic activity, J. Phys. Chem. c. 117 (46) (2013) 24601–24610, https://doi.org/10.1021/jp408627e.

[16] C. Lee, S. Jeong, N. Myung, K. Rajeshwar, Preparation of Au-Bi_2O_3 nanocomposite by anodic electrodeposition combined with galvanic replacement, J. Electrochem. Soc. 161 (10) (2014) D499–D503, https://doi.org/10.1149/2.0421410jes.

[17] J. Ke, C. Zhao, H. Zhou, X. Duan, S. Wang, Enhanced solar light driven activity of p-n heterojunction for water oxidation induced by deposition of Cu_2O on Bi_2O_3 microplates, Sustain. Mater. Techno. 19 (2019) e00088.

[18] B. Xu, Y. An, Y. Liu, X. Qin, X. Zhang, Y. Dai, Z. Wang, P. Wang, M.-H. Whangbo, B. Huang, Enhancing the photocatalytic activity of BiOX (X = Cl, Br, and I), (BiO)2CO3 and Bi2O3 by modifying their surfaces with polar organic anions, 4-substituted thiophenolates, J. Mater. Chem. A. 5 (27) (2017) 14406–14414, https://doi.org/10.1039/c7ta03970k.

[19] Y.-P. Yuan, S.-W. Cao, L.-S. Yin, L. Xu, C. Xue, NiS_2 Co-catalyst decoration on $CdLa_2S_4$ nanocrystals for efficient photocatalytic hydrogen generation under visible light irradiation, Int. J. Hydrogen. Energy. 38 (18) (2013) 7218–7223, https://doi.org/10.1016/j.ijhydene.2013.03.169.

[20] J. Hou, C. Yang, Z. Wang, S. Jiao, H. Zhu, Hydrothermal synthesis of CdS/$CdLa_2S_4$ heterostructures for efficient visible-light-driven photocatalytic hydrogen production, RSC Adv. 2 (27) (2012) 10330–10336, https://doi.org/10.1039/c2ra21641h.

[21] X. Liu, X. Chen, S. Wang, L. Yan, J. Yan, H. Guo, F. Yang, J. Lin, Promoting the photocatalytic $_H$2 evolution activity of CdL_a2_S4 nanocrystalline using few-layered W_S2 nanosheet as a co-catalyst, Int. J. Hydrogen. Energy. 47 (4) (2022) 2327–2337, https://doi.org/10.1016/j.ijhydene.2021.10.227.

[22] Y. Luo, H. Chen, X. Li, Z. Gong, X. Wang, X. Peng, M. He, Z. Sheng, Wet chemical synthesis of Bi_2S_3 nanorods for efficient photocatalysis, Mater. Lettl. 105 (2013) 12–15, https://doi.org/10.1016/j.matlet.2013.04.006.

[23] D. Liu, W. Cao, F. Li, Y. Hu, Y. Ding, Controllable morphology engineering of Cu_2O nanoparticles for non-enzymatic glucose sensing, Microchem. J. 193 (2023) 108922, https://doi.org/10.1016/j.microc.2023.108922.

[24] S. Sun, X. Zhang, Q. Yang, S. Liang, X. Zhang, Z. Yang, Cuprous oxide (Cu2O) crystals with tailored architectures: A comprehensive review on synthesis, fundamental properties, functional modifications and applications, Prog. Mater. Sci. 96 (2018) 111–173, https://doi.org/10.1016/j.pmatsci.2018.03.006.

[25] B.A. Koiki, O.A. Arotiba, Cu_2O as an emerging semiconductor in photocatalytic and photoelectrocatalytic treatment of water contaminated with organic substances: a review, RSC Adv. 10 (60) (2020) 36514–36525, https://doi.org/10.1039/d0ra06858f.

[26] H. Qin, X. Zhao, H. Zhao, L. Yan, W. Fan, Well-organized CN-M/CN-U/Pt-TiO_2 ternary heterojunction design for boosting photocatalytic H2 production via electronic continuous and directional transmission, Appl. Catal. A-Gen. 576 (2019) 74–84, https://doi.org/10.1016/j.apcata.2019.03.002.

[27] J. Peng, Z. Zheng, H. Tan, J. Yang, D. Zheng, Y. Song, F. Lu, Y. Chen, W. Gao, Rational design of ZnIn2S4/CdIn2S4/CdS with hollow heterostructure for the sensitive determination of carbohydrate antigen 19–9, Sensor. Actuat. B-Chem. 363 (2022) 131863, https://doi.org/10.1016/j.snb.2022.131863.

[28] W. Luo, F. Li, Q. Li, X. Wang, W. Yang, L. Zhou, L. Mai, Heterostructured Bi_2S_3-Bi_2O_3 Nanosheets with a Built-In Electric Field for Improved Sodium Storage, ACS Appl. Mater. Interfaces. 10 (8) (2018) 7201–7207, https://doi.org/10.1021/acsami.8b01613.

[29] T.Y. Liang, S.J. Chan, A.S. Patra, P.L. Hsieh, Y.A. Chen, H.H. Ma, M.H. Huang, Inactive Cu_2O cubes become highly photocatalytically active with Ag_2S deposition, ACS Appl. Mater. Interfaces. 13 (9) (2021) 11515–11523, https://doi.org/10.1021/acsami.1c00342.

[30] Q. Chen, J. Li, L. Cheng, H. Liu, Construction of CdLa2S4/MIL-88A(Fe) heterojunctions for enhanced photocatalytic H2-evolution activity via a direct Z-scheme electron transfer, Chem. Eng. J. 379 (2020) 122389, https://doi.org/10.1016/j.cej.2019.122389.

[31] F.X. Wang, C. Ye, S. Mo, H.Q. Luo, J.R. Chen, Y. Shi, N.B. Li, Enhanced photoelectrochemical sensing based on novel synthesized Bi_2S_3@Bi_2O_3 nanosheet heterostructure for ultrasensitive determination of l-cysteine, Anal. and Bioanal. Chem. 411 (14) (2019) 3059–3068, https://doi.org/10.1007/s00216-019-01765-7.

[32] H. Shi, Y. Zhao, J. Fan, Z. Tang, Construction of novel Z-scheme flower-like Bi2S3/SnIn4S8 heterojunctions with enhanced visible light photodegradation and bactericidal activity, Appl. Surf. Sci. 465 (2019) 212–222, https://doi.org/10.1016/j.apsusc.2018.09.164.

[33] Q. Cai, H. Li, W. Dong, G. Jie, Versatile photoelectrochemical biosensor based on AIS/ZnS QDs sensitized-WSe_2 nanoflowers coupled with DNA nanostructure probe for"On−Off" assays of TNF-α and MTase, Biosens. Bioelectron. 241 (2023) 115704, https://doi.org/10.1016/j.bios.2023.115704.

[34] R. Ge, X. Lin, H. Dai, J. Wei, T. Jiao, Q. Chen, M. Oyama, Q. Chen, X. Chen, Photoelectrochemical sensors with near-infrared-responsive reduced graphene oxide and MoS_2 for quantification of escherichia coli O157:H7, ACS Appl. Mater. Interfaces. 14 (36) (2022) 41649–41658, https://doi.org/10.1021/acsami.2c13292.

[35] D. Choi, C. Zhu, S. Fu, D. Du, M.H. Engelhard, Y. Lin, Electrochemically controlled ion-exchange property of carbon nanotubes/polypyrrole nanocomposite in various electrolyte solutions, Electroanal. 29 (3) (2016) 929–936, https://doi.org/10.1002/elan.201600466.

[36] J.T. Cao, J.L. Lv, X.J. Liao, S.H. Ma, Y.M. Liu, A membraneless self-powered photoelectrochemical biosensor based on Bi_2S_3/$BiPO_4$ heterojunction photoanode coupling with redox cycling signal amplification strategy, Biosens. Bioelectron. 195 (2022) 113651, https://doi.org/10.1016/j.bios.2021.113651.

[37] J. Chen, N. Song, N. Zhang, Z. Gao, D. Wu, H.M.X. Ren, Q. Wei, Smartphone-controlled portable photoelectrochemical immunosensor for point-of-care testing

of carcinoembryonic antigen, Chem. Eng. J. 473 (2023) 145276, https://doi.org/10.1016/j.cej.2023.145276.
[38] Y. Hou, J. Chen, B. Xie, T. Li, M. Yang, Electrochemical assay for analysis of circulation tumor cells based on isolation of the cell with magnetic nanoparticles and reaction of DNA with molybdate, Mikrochim. Acta. 187 (7) (2020) 420, https://doi.org/10.1007/s00604-020-04395-4.
[39] X. Zhong, X. Li, Y. Zhuo, Y. Chai, R. Yuan, Synthesizing anode electrochemiluminescent self-catalyzed carbon dots-based nanocomposites and its application in sensitive ECL biosensor for microRNA detection, Ssensors. Actuat. b: Chem. 305 (2020) 127490, https://doi.org/10.1016/j.snb.2019.127490.
[40] Q. Cai, H. Li, B. Wang, G. Jie, A spatial-potential-resolved electrochemiluminescence biosensor for simultaneous detection of BRCA1 and BRCA2 based on a novel self-luminescent metal–organic framework, Chem. Eng. J. 476 (2023) 146799, https://doi.org/10.1016/j.cej.2023.146799.